PAPER

Check for updates

Investigation of coal pore structure evolution under temperature–time coupling using low-field nuclear magnetic resonance

Ziwen Dong,[ab] Haojie Zhang, [ID] *[abc] Xian Wu,[c] Ronghao Xu[c] and Song Kong[ab]

To investigate the coupled effects of temperature and time on the evolution of coal pore structure, this study employed low-field nuclear magnetic resonance (LF-NMR) combined with oil bath heat treatment experiments to systematically characterize variations in T_2 relaxation spectra, pore size distribution, throat structure, and porosity in coal samples. The experimental findings demonstrate that the T_2 spectra of all coal samples display a bimodal distribution, wherein micropores represent the predominant pore type, whereas macropores and fractures remain predominantly undeveloped. After heat treatment, the micropore peak intensity decreased and shifted to a lower value, indicating pore contraction or collapse. At 35 °C, the pore-throat volume and porosity exhibit characteristics of a dynamic equilibrium, showing partial recovery after an initial short-term contraction. In contrast, at 65 °C, the thermal stress induced by differential thermal expansion exceeds the strength of the coal matrix, resulting in the irreversible collapse of micropores and a monotonic decrease in porosity. Submicron-sized pore throats (<0.1 μm) exhibited higher sensitivity to the coupled effects of temperature and time, whereas macropore throats remained largely unaffected. Furthermore, this study reveals that the coupled temperature–time effect primarily governs the irreversible damage processes in the micropore-throat system through a thermal stress mechanism. This, in turn, modulates the coal's oxidative activity and spontaneous combustion (SC) propensity, thereby providing a critical theoretical foundation for the early prediction and warning of coal spontaneous combustion (CSC), as well as for the development of targeted inhibition and control strategies.

1. Introduction

CSC is one of the primary hazards threatening coal mine safety. It is fundamentally a low-temperature exothermic oxidation process triggered by the interaction between coal and oxygen.[1–3] This process is governed by the pore structure, wherein micropores serve as the primary adsorption sites, and their connectivity directly influences the efficiency of oxygen transport. Under deep mining conditions, coal seams are persistently subjected to geothermal environments ranging from 35 to 65 °C. Temperature-induced cumulative thermal stress alters pore structural characteristics, thereby accelerating the progression of SC.[4–6] Therefore, investigating the dynamic evolution of coal pore structure under the coupled effects of temperature and time, along with its influence mechanism on oxidation activity, holds significant value for accurately predicting the risk of CSC,

developing efficient inhibition technologies, and ensuring mine safety.

Current techniques for characterizing coal pore structures primarily include mercury intrusion porosimetry (MIP), low-temperature nitrogen adsorption (BET), and micro-computed tomography (micro-CT).[7,8] These conventional methods exhibit certain limitations. For instance, mercury intrusion porosimetry (MIP) applies high pressure that may compress the microporous structure. The gas adsorption method lacks sufficient resolution for pores larger than 100 nanometers. Although micro-computed tomography (micro-CT) enables three-dimensional reconstruction of the pore network, its resolution is typically constrained to the micrometer scale, thereby limiting the accurate detection of sub-micrometer pore throat variations. In contrast, the LF-NMR technology, with its advantages of non-destructive detection and full-pitch coverage, has become an effective means for dynamic characterization. In recent years, both domestic and international scholars have conducted research and systematic analyses on the pore structure characteristics of coal from various perspectives. Zhao *et al.*[9] investigated the pore structure of coal using techniques such as mercury intrusion porosimetry and low-temperature nitrogen adsorption. Their findings revealed that an increase

aSchool of Materials and Chemical Engineering/School of Safety Engineering, Ningbo University of Technology, Ningbo, Zhejiang 315211, China

bZhejiang Institute of Tianjin University, Ningbo, Zhejiang 315211, China

cSchool of Safety Science and Engineering, Liaoning Technical University, Fuxin, Liaoning 123000, China. E-mail: 1941144168@qq.com

in temperature led to a higher fractal dimension of large pores, indicating more developed pore structures. Conversely, the fractal dimension of small pores was observed to decrease with rising temperature. Meng et al.[10] employed a molecular-scale reconstruction method to investigate coal pore structures and proposed that with increasing coal metamorphic grade, the specific surface area and pore volume initially decrease and subsequently increase, while the pore quantity exhibits a tri-phasic growth pattern characterized by rapid, followed by slow, and then rapid increments. Jia[11] employed scanning electron microscopy to demonstrate that low-rank coal exhibits abundant pore development with superior connectivity. Additionally, mercury intrusion porosimetry and low-temperature nitrogen adsorption experiments confirmed that the specific surface area of micropores predominantly contributes to the total pore surface area, serving as the principal adsorption sites for methane in low-rank coal. Nan et al.[12] applied CT scanning technology to achieve quantitative characterization of coal's microstructure and to visualize the seepage behavior within macropores. Their analysis indicated that abrupt reductions in pore radius in specific regions of the pore structure led to a marked enhancement in seepage velocity. Wang et al.[13] investigated the impact of mixed acid solutions on the pore structure of high-rank coal using LF-NMR combined with static dissolution experiments. Their results revealed that the size, quantity, and volume of all pore types in the distilled water-treated coal samples exhibited a consistent reduction. Zhu et al.[14] employed mercury intrusion porosimetry (MIP) and low-temperature nitrogen gas adsorption (N$_2$GA), in combination with LF-NMR experiments, to systematically investigate the pore structure characteristics of coal. Their results demonstrated that the total porosity first decreases and then increases with increasing coalification degree. Hu et al.[15] employed LF-NMR technology to investigate the evolution of water states during the wetting process of coal particles. Their observations indicated that a reduction in particle size was associated with an increase in the proportion of transition pores and micropores. However, it was also found that when the particle size was either excessively large or excessively small, the fractal characteristics of these pores became less distinct. Yang et al.[16] conducted mercury injection, liquid nitrogen adsorption, and nuclear magnetic resonance experiments, along with other methodologies, to systematically investigate the pore characteristics of middle-rank coal reservoirs. Their findings revealed that with increasing coal rank, the proportion of medium-to large-sized pores and flowing pore throats progressively decreases. This is accompanied by a deterioration in pore connectivity, ultimately leading to a systematic reduction in permeability. Li et al.[17] observed that with the increase in air pressure, the proportion of small pores in the coal-rock first increased and subsequently decreased, the connectivity of pore throats and fractures improved, and the proportion of medium-to large-sized pores initially decreased and then increased.

Most of the aforementioned studies have concentrated on the effects of varying coal ranks and metamorphic degrees on the pore structure of coal. However, the majority of existing studies have primarily concentrated on coal pore responses under single temperature conditions or transient thermal effects. A systematic understanding of the underlying mechanisms by which the coupled effects of temperature and time cooperatively govern the dynamic evolution of pore structure over prolonged exposure periods remains limited. Accordingly, this study employs a LF-NMR system to investigate the temporal evolution of pore structures in coal samples subjected to varying temperatures and durations. The research aims to establish a theoretical framework elucidating the effects of temperature and time on coal pore structures, thereby offering a novel perspective for the prevention and control of SC.

2. Experimental approaches

2.1 Coal samples preparation

For this experiment, the coal samples were obtained from the bituminous coal seam at Yilan No. 3 Coal Mine in Yilan County, Heilongjiang Province. Fresh, large bulk samples were collected, immediately packaged in sealed bags, and transported to the laboratory for analysis. A batch of cylindrical coal cores (25 mm in diameter × 50 mm in height) was drilled using an automatic coring machine. All experimental samples were derived from the same raw coal block to ensure sample homogeneity. The drilled coal cores were initially screened to select specimens with a homogeneous texture, regular geometry, and no surface fissures for subsequent experiments. The results of the proximate analysis of the coal samples are presented in Table 1.

2.2 Experimental procedures

(1) The experimental procedure commenced with an oil bath heat treatment of the coal samples. The selected samples were loaded into glass test tubes, with five specimens per tube, and hermetically sealed to prevent contamination or moisture exchange. These sealed tubes were then placed in two independent HH-350 oil baths, each maintaining a temperature control accuracy of ±0.5 °C, and subjected to different thermal treatment conditions. Silicone oil was employed as the heating medium due to its high specific heat capacity, which facilitates rapid and uniform heat transfer, thereby ensuring consistent and stable thermal distribution throughout the experiment. Detailed treatment parameters and corresponding sample designations are summarized in Table 2. Upon completion of the designated treatment duration, the tubes were removed from the oil baths and allowed to cool naturally to ambient temperature over a period of 0.5 to 1 hour. Once cooled, the coal samples were retrieved and immediately transferred into airtight containers for subsequent characterization and analysis.

(2) Nuclear magnetic resonance analysis. The pore structure of the coal samples was characterized using an NMI20-040V-I

Table 1 Industrial analysis results of coal samples

M (ad)/%	A (ad)/%	V (ad)/%	FC (ad)/%
9.58	5.08	39.50	45.84

Table 2 Processing methods and nomenclature of coal samples

Processing methods and nomenclature of coal samples

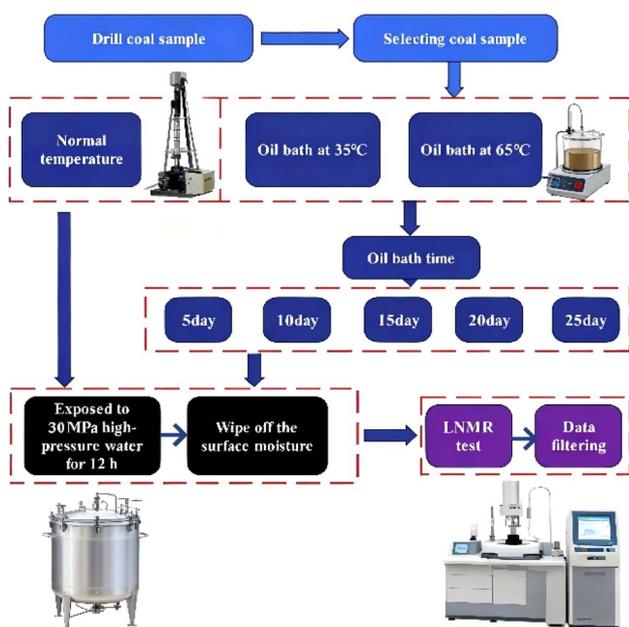| Oil bath time	Oil bath temperature	Notation
—	—	RC
5 day	35 °C	M1
10 day		M2
15 day		M3
20 day		M4
25 day		M5
5 day	65 °C	M6
10 day		M7
15 day		M8
20 day		M9
25 day		M10

Fig. 1 Schematic flowchart of the experimental procedure.

LF-NMR analyzer. The specific procedure was as follows: The heat-treated coal samples were first saturated by immersion in water pressurized to 30 MPa for 12 hours. Subsequently, surface moisture was gently blotted off with absorbent paper, and the samples were then promptly transferred to the NMI20-040V-I system for LF-NMR measurement. A schematic flowchart of the experimental procedure is presented in Fig. 1.

(3) Data screening. The data from coal samples that completed LF-NMR testing were screened. Three parallel coal samples with comparable porosity were selected from each group for subsequent analysis to ensure data reliability.

3. Results and analysis

3.1 T_2 relaxation spectrum analysis

Nuclear magnetic resonance (NMR) technology primarily analyzes the distribution of relaxation times in time-domain signals to probe interactions between molecules.[18,19] This technique enables the determination of the T_2 distribution of water within the pores of fully water-saturated coal samples. The relationship between the transverse relaxation time (T_2) and the internal pore radius (r_c) is presented in eqn (1):

$$\frac{1}{T_2} = \rho_2\left(\frac{S}{V}\right) = F_s\left(\frac{\rho_2}{r_c}\right) \tag{1}$$

where T_2 is the transverse relaxation time, ms; ρ_2 is the surface relaxivity, μm ms^{-1}; S is the pore surface area, μm^2; V is the pore volume, μm^3; F_s is the pore shape factor ($F_s = 3$ for spherical pores, $F_s = 2$ for cylindrical pores, and $F_s = 1$ for slit-shaped pores); and r_c is the pore radius, nm.

The relationship between the pore radius r_c of the coal samples and the transverse relaxation time T_2 is presented in eqn (2):

$$r_c = \alpha T_2 \tag{2}$$

where α is a conversion factor, $\alpha = F_s\rho_2$.

As indicated by eqn (2), a positive correlation exists between the transverse relaxation time (T_2) and the pore radius of coal samples. Specifically, a longer T_2 value corresponds to a larger pore size, a higher signal amplitude, and consequently, a greater abundance of such pores. The area under the T_2 distribution curve reflects the relative proportion of pores and fractures within the coal sample, whereas the number and width of the peaks provide effective indicators of the distribution and connectivity of the internal pore structure.[20,21] The T_2 distribution curves of water-saturated coal samples treated under varying temperature and duration conditions are shown in Fig. 2.

With ref. 22 to the pore classification method established in the literature, pores were categorized based on their T_2 relaxation times as follows: micropores (0.01–1 ms), mesopores (1–10 ms), macropores (10–100 ms), and fractures/large pores (100–10000 ms). As shown in Fig. 2, the T_2 distribution curves of the experimental coal samples exhibit a bimodal pattern. The relaxation times corresponding to the peak values fall within the ranges of 0.1–10 ms and 20–100 ms, respectively, with the majority of T_2 signals being primarily concentrated in the 0.1–10 ms interval. Analysis of the T_2 distribution curves reveals that the short relaxation time component dominates the spectrum, suggesting that the pore structure of the experimental coal samples consists predominantly of micropores and mesopores, with macropores and fractures being poorly developed. Furthermore, the lack of continuity between the two peaks indicates relatively poor pore connectivity.

3.2 Pore size distribution characteristics

LF-NMR was utilized to perform non-destructive scanning tests on raw coal samples and those subjected to thermal treatment under varying temperatures and durations. The acquired NMR signals were processed and transformed into pore size distribution profiles, representing distinct pore size intervals, as illustrated in Fig. 3. The suffixes −1, −2, and −3 denote parallel replicate samples. According to the Hodot classification
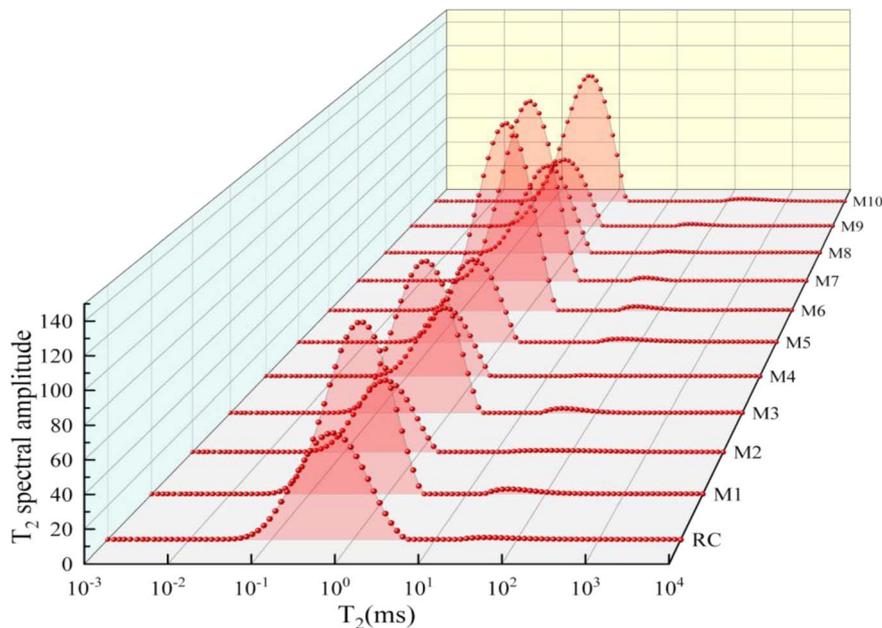
Fig. 2 T_2 distribution curves of water-saturated coal samples under varied temperature and time conditions.

method, the pore structure of coal is categorized into four types based on diameter: micropores (<10 nm), mesopores (10–100 nm), macropores (100–1000 nm), and fractures (>1000 nm).[23] Among these, micropores serve as the primary space for adsorbed gas storage in coal seams. Mesopores act as crucial bridges connecting micropores to larger-scale pores, playing a key role in gas diffusion processes. In contrast, free gas within the coal seam is predominantly stored in the macropore structure.

The Fig. 4 illustrates the average pore size distribution of both raw coal and samples treated under various temperature and time conditions. As revealed by the figure, the pore size distribution is predominantly concentrated within the ranges of 0.0015–0.08 μm and 0.1–2.9 μm. This indicates a pore structure dominated by micropores and mesopores, with a limited development of macropores and negligible presence of fractures. Compared to raw coal, the heat-treated coal sample exhibits a reduced peak value in micropores, with the peak shifting leftward. This suggests that the micropores may have experienced contraction or collapse. Meanwhile, under the two temperature conditions of 35 °C and 65 °C, the pore size distribution demonstrates complex and divergent evolutionary trends with prolonged heat treatment duration. Specifically, in the 35 °C treatment group, the pore size distribution curve exhibits a distinct peak at approximately 0.006 μm, with its intensity demonstrating a fluctuant decline as the treatment duration increases. Taking coal samples M1 through M5 as examples, their peak values were 0.38%, 0.22%, 0.28%, 0.21%, and 0.26%, respectively. The highest value was recorded at 5 days (M1), while the lowest occurred at 20 days (M4). In contrast, under the 65 °C condition, the micropore peak intensity at 5 days (M6) was 15.3% lower than that of the 35 °C counterpart (M1), exhibiting a monotonically decreasing trend

with prolonged treatment. By day 25 (M10), the peak intensity had decreased by 40% compared to its initial state (M6), resulting in a cumulative reduction of 55.2%. Furthermore, the secondary peak within the 0.1–0.3 μm range in this treatment group remained relatively stable from days 5 to 15 (M6–M8), however, it exhibited notable attenuation during days 20 to 25 (M9–M10), suggesting that prolonged pyrolysis also induced partial degradation of the mesoporous structure.

3.3 Pore throat structure characterization results

Pore throats refer to the narrowest constrictions between interconnected pores and, together with the pores themselves, collectively form the pore structure of coal. The size of pore throats governs the lower limit of effective pore size in connectable pores, and their distribution directly dictates overall pore connectivity.[24–26] According to research, pore throats are classified into three categories by size: 0–0.25 μm as micropore throats, 0.25–1 μm as meso-macropore throats, and greater than 1 μm as fractures. The proportional distribution of pore throat sizes in coal samples treated under different temperature and duration conditions is presented in Table 3.

Based on the analysis of coal pore structure evolution mechanisms, the pore throat structure exhibits significant scale-selective modification during heat treatment, with its size distribution following the relationship shown in eqn (3):

$$r_h = \frac{2\gamma \cos \theta}{P_c} \quad (3)$$

where r_h is the pore throat radius, μm; γ is the liquid–solid interfacial tension, N m^{-1}; θ is the contact angle; P_c and is the capillary pressure, MPa. The distribution of pore throats in coal samples under various temperature and duration conditions is presented in Fig. 5.
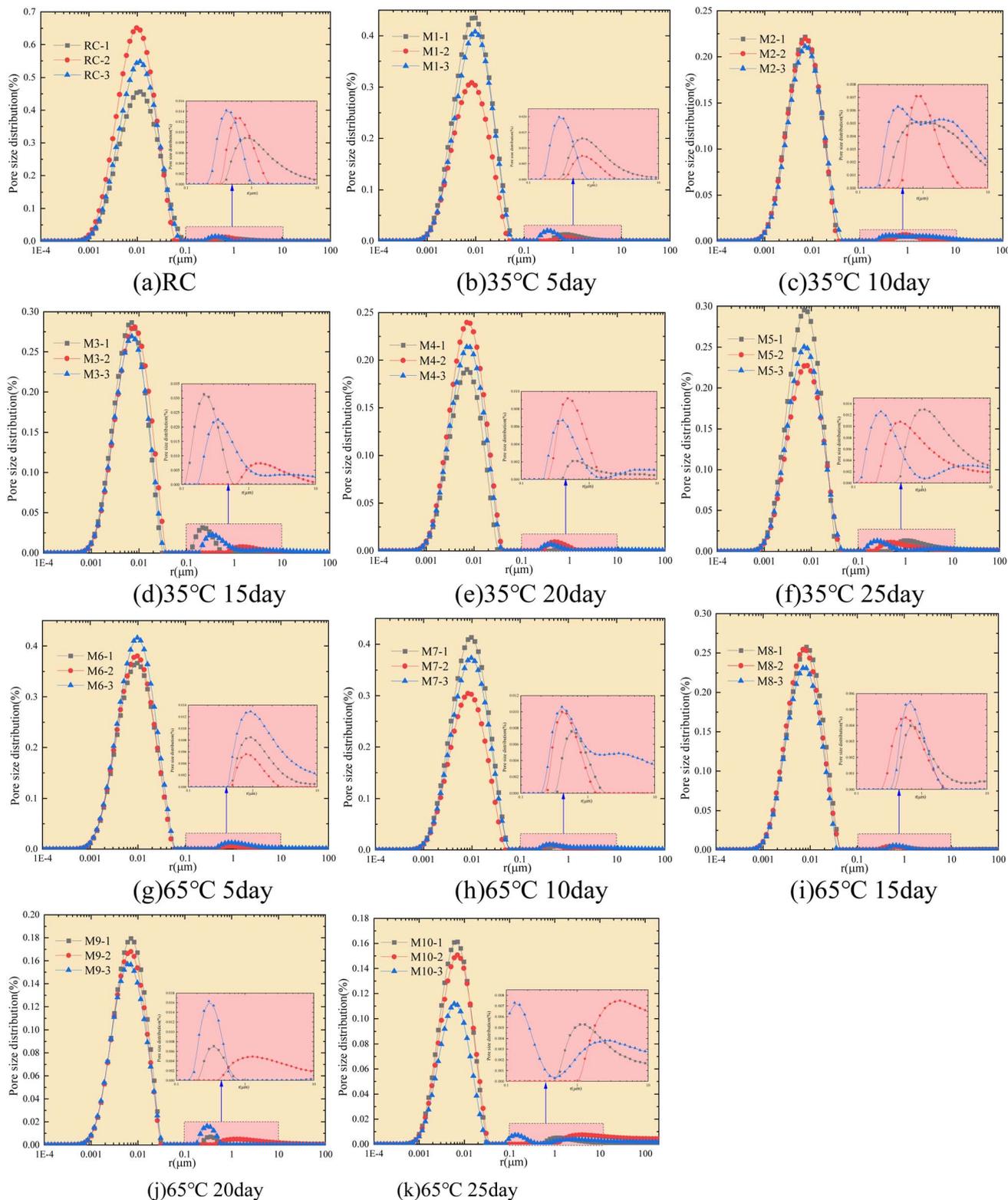
Fig. 3 Pore size distribution of coal samples under varied temperature and time conditions.

As observed in the figure, pore throat distribution values are notably higher within the 0–0.1 μm aperture range and are significantly more densely distributed compared to the $r > 0.1$ μm region. This indicates that the experimental coal samples contain abundant micropores with well-developed pore throats, and exhibit superior connectivity compared to *meso*-macropores. Furthermore, data analysis from Table 3 and Fig. 4 indicates that compared to raw coal, all heat-treated coal
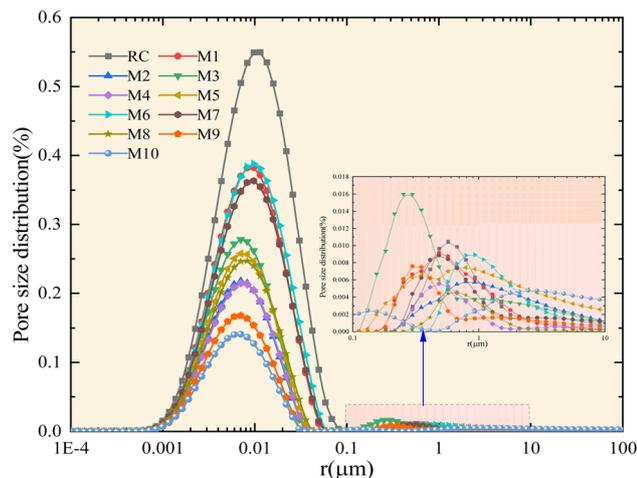
Fig. 4 Average pore size distribution of water-saturated coal samples under varied temperature and time conditions.

Table 3 The proportion of pore throats in coal samples under different temperature and time conditions

Notation	Micropore throats (%)	Meso-macropore throats (%)	Fractures (%)	Overall (%)
RC	7.60	0.06	0.02	7.68
M1	5.04	0.07	0.02	5.13
M2	2.65	0.03	0.05	2.73
M3	3.38	0.08	0.04	3.50
M4	2.63	0.03	0.01	2.67
M5	3.20	0.06	0.05	3.31
M6	5.20	0.03	0.05	5.28
M7	4.81	0.06	0.03	4.90
M8	3.12	0.02	0.01	3.15
M9	2.02	0.04	0.02	2.08
M10	1.70	0.01	0.28	1.99

samples exhibit a reduced proportion of micropore throats. Specifically, in the 35 °C treatment group, the proportion of micropore throats exhibited a nonlinear decreasing trend with prolonged treatment duration (M1: 5.04% → M2: 2.65% → M3: 3.38% → M4: 2.63% → M5: 3.20%), reaching its minimum value at 20 days (M4). This fluctuating pattern may be attributed to the contraction effect resulting from dehydration of clay minerals in coal under low-temperature conditions: $Al_2Si_2O_5(OH)_4 \xrightarrow{35\ °C} Al_2Si_2O_7 + 2H_2O$. Moisture loss induces pore throat contraction, while partial structural support from mineral recrystallization creates a dynamic equilibrium

between these processes, leading to the proportional recovery observed in M3 and M5. In contrast, the 65 °C treatment group exhibited a monotonically decreasing trend over time. After 25 days of treatment (M10), the proportion of micropore throats decreased to 1.70%, representing a 67.3% reduction compared to the short-duration sample at the same temperature (M6), and a cumulative decrease of 77.6% relative to the raw coal. Notably, under prolonged 65 °C treatment (25 days, M10), the proportion of fractures (>1 μm) abnormally increased to 0.28%, significantly higher than that of other samples (generally <0.05%). Integrated with the pronounced peak observed in the $r > 1$ μm region for sample M10 in Fig. 5, it can be inferred that prolonged high-temperature treatment amplifies the differential thermal expansion coefficients between organic and mineral
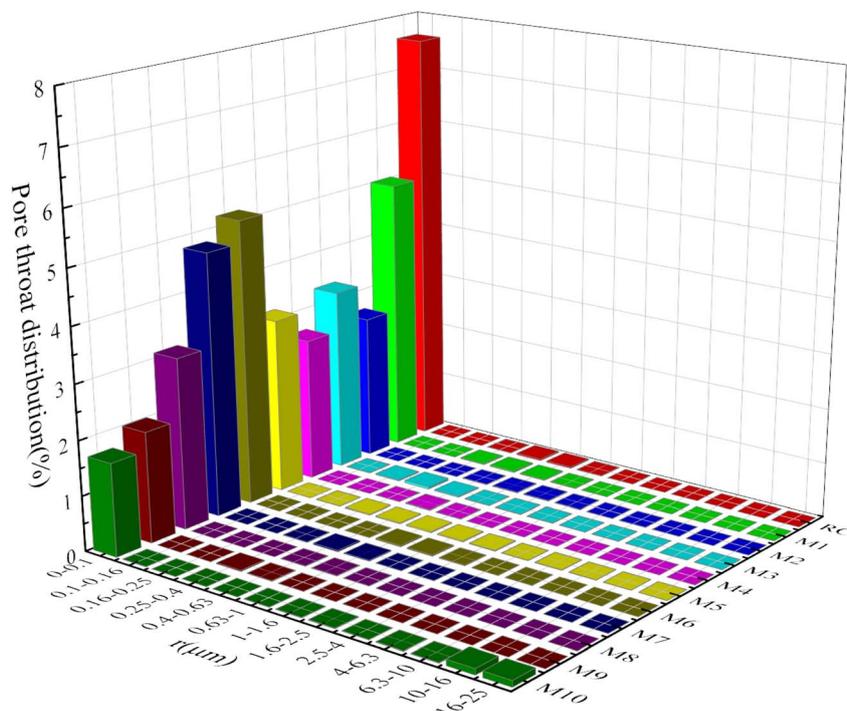

Fig. 5 Pore throat distribution in coal samples under different temperature and time conditions.

Table 4 Porosity of coal samples under different temperature and time conditions

Notation	Parallel coal sample notation	Porosity (%)	Average porosity (%)
RC	RC-1	6.66	7.69
	RC-2	8.83	
	RC-3	7.58	
M1	M1-1	5.94	5.13
	M1-2	4.05	
	M1-3	5.4	
M2	M2-1	2.77	2.73
	M2-2	2.71	
	M2-3	2.72	
M3	M3-1	3.53	3.51
	M3-2	3.55	
	M3-3	3.45	
M4	M4-1	2.27	2.68
	M4-2	3.05	
	M4-3	2.71	
M5	M5-1	3.78	3.36
	M5-2	3.05	
	M5-3	3.26	
M6	M6-1	5.01	5.30
	M6-2	5.13	
	M6-3	5.76	
M7	M7-1	4.03	4.33
	M7-2	5.12	
	M7-3	3.84	
M8	M8-1	3.32	3.16
	M8-2	3.24	
	M8-3	2.92	
M9	M9-1	2.38	2.21
	M9-2	2.18	
	M9-3	2.08	
M10	M10-1	2.02	1.83
	M10-2	2.01	
	M10-3	1.45	

Fig. 6 Cumulative porosity of coal samples under various temperature and time conditions.

components within the coal matrix. This thereby induces localized thermal stress concentration, ultimately exceeding the coal's tensile strength and initiating fracture development. The proportion of *meso*-macropore throats (0.25–1 μm) in all experimental samples remained at an extremely low level (<0.1%), showing no discernible trend with variations in temperature or treatment duration. This clearly indicates that heat treatment exerts significant scale-selective effects on the pore structure of the coal matrix, particularly in terms of modifying the seepage.

3.4 Porosity

As a heterogeneous porous medium, coal develops internal thermal stress ($\sigma_{thermal}$) due to differential thermal expansion coefficients among its components (organic matter/minerals), as shown in eqn (4):

$$\sigma_{thermal} = E \cdot \Delta\alpha \cdot \Delta T \tag{4}$$

where E is the elastic modulus of coal, MPa; α is the coefficient of thermal expansion, K^{-1}; ΔT is the temperature increase, K.
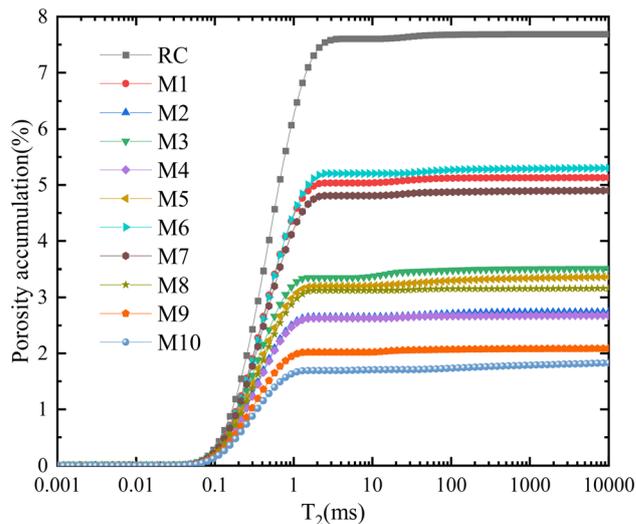
Analysis of porosity evolution characteristics presented in Table 4 and Fig. 6 indicates that the coupled effects of temperature and time significantly influenced the pore structure of coal samples. Compared to raw coal, all heat-treated coal samples exhibited reduced porosity, yet their evolution patterns demonstrated distinct temperature dependence. Under 35 °C conditions, porosity exhibited a nonlinear fluctuating decline with prolonged treatment duration. An abrupt reduction occurred in the short term (≤10 days), driven primarily by pore throat contraction (mainly due to clay mineral dehydration), whereas during extended treatment, stress release facilitated the reopening of partially closed pores. This process established a dynamic equilibrium between contraction and re-expansion, resulting in a modest recovery of porosity. Under 65 °C conditions, however, thermal stress induced by pronounced differential thermal expansion (increased ΔT) exceeded the strength of the coal matrix, resulting in a monotonically decreasing trend in porosity with prolonged treatment duration, accompanied by an accelerating rate of decline. This process is primarily characterized by the irreversible collapse of micropores. Even though localized thermal stress concentration induced fracture formation during the later stage (25 days) (see Table 3), the newly created pore volume failed to compensate for the pore loss resulting from micropore collapse.

4. Conclusions

Using LF-NMR technology, this study systematically investigated the coupled effects of temperature (35 °C and 65 °C) and time (5–25 days) on the pore size distribution, pore throats, and porosity of bituminous coal. The research reveals the dynamic evolution mechanisms of coal pore structure under coupled temperature–time conditions. The main conclusions are as follows:

(1) The T_2 distribution curves of coal samples treated at different temperatures and durations all exhibited a bimodal

structure. The pore system was predominantly composed of micropores, with relatively fewer mesopores, while macropores and fractures remained largely undeveloped. The two pore peaks exhibit a lack of continuity, indicating poor connectivity within the coal sample. Heat treatment results in a reduction of the micropore peak intensity and a shift toward shorter relaxation time values, indicating structural contraction or collapse of the micropore system.

(2) Under the 35 °C treatment condition, both pore-throat volume and porosity exhibited non-monotonic evolution characteristics, characterized by a dynamic equilibrium process of partial recovery following initial rapid contraction. This pattern reflects the competitive mechanism between clay mineral dehydration and organic matter stress release within the coal. However, under the 65 °C experimental condition, micro-pore collapse induced by differential thermal expansion becomes the dominant mechanism. The resulting damage cannot be offset by the subsequent development of fractures, leading to a continuous reduction in total pore volume. Consequently, both pore throat dimensions and overall porosity exhibit a synchronous and irreversible decline.

(3) The pore throat distribution is predominantly localized within the sub-micron scale (<0.1 μm), where the reduction in pore volume constitutes the primary contributor to the observed decline in overall porosity. In contrast, the larger-sized pores exhibited minimal response to the coupled effects of temperature and time, suggesting that the modification of seepage channels is constrained by the critical size effect inherent in the micropore throat system.

(4) This study reveals pore structure evolution patterns, particularly the two distinct modes of "dynamic equilibrium" at 35 °C and "irreversible collapse" at 65 °C, providing new structural perspectives for understanding how temperature–time coupling effects modulate the potential mechanisms of coal spontaneous combustion propensity. It is well established that pores serve as the primary sites for gas adsorption and diffusion. Based on findings, it can be reasonably inferred that the dynamic pore structure changes observed at 35 °C may intermittently affect the opening and closing of oxygen diffusion pathways, thereby exerting complex modulation on the oxidative activity of the coal mass. At 65 °C, the irreversible collapse of micropores and the sustained reduction in porosity may fundamentally impair oxygen transport and adsorption capacities, while simultaneously altering the retention environment for reaction products. These pore structure-driven effects are likely to represent key structural determinants underlying the complex variations in coal's propensity for spontaneous combustion. In subsequent research, this hypothesis will be empirically validated through direct correlations between pore structural parameters and gas adsorption or reactivity measurements.

Author contributions

Ziwen Dong: writing – original draft; data analysis and writing – original draft. Haojie Zhang: investigation; writing – review & editing; funding acquisition. Xian Wu: investigation; formal analysis. Ronghao Xu: methodology; supervision. Song Kong: resources; project administration.

Conflicts of interest

The authors declare no competing financial interest.

Data availability

All relevant data are within the paper.

Acknowledgements

References

1 J. Li, J. Sun, Z. Yang, *et al.*, Different perspectives and explanations regarding the influence of pre-oxidation on the spontaneous combustion characteristics of coal, *J. China Univ. Min. Technol.*, 2025, **54**, 423–436.

2 H. Liu, Z. Li, Y. Yang, *et al.*, Study on the thermal behavior of coal during the spontaneous combustion latency, *Energy*, 2023, **281**, 128292.

3 H. Yan, B. Nie, F. Kong, *et al.*, Experimental investigation of coal particle size on the kinetic properties of coal oxidation and spontaneous combustion limit parameters, *Energy*, 2023, **270**, 126890.

4 M. Yan, F. Yang, B. Zhang, *et al.*, Influence of Pore Structure Characteristics of Low Permeability Coal on Gas Nonlinear Seepage, *Nat. Resour. Res.*, 2024, **33**, 1209–1225.

5 M. Yan, B. Zhang, J. Li, *et al.*, Research on influence of pore structure connectivity of low gas permeability on coal seam permeability, *Saf. Coal Mine*, 2021, **52**, 31–38.

6 G. Wang, J. Shen, S. Liu, *et al.*, Three-dimensional modeling and analysis of macro-pore structure of coal using combined X-ray CT imaging and fractal theory, *Int. J. Rock Mech. Min. Sci.*, 2019, **123**, 104082.

7 T. Wang, Z. Deng, H. Hu, *et al.*, Pore structure of deep coal of different ranks and its effect on coalbed methane adsorption, *Int. J. Hydrogen Energy*, 2024, **59**, 144–158.

8 H. Gong, D. Li, Z. Li, *et al.*, Study on mechanical properties and crack propagation of coal specimen based on CT scanning technology, *J. Min. & Saf. Eng.*, 2024, **41**, 612–622.

9 S. Zhao, X. Chen, X. Li, *et al.*, Experimental analysis of the effect of temperature on coal pore structure transformation, *Fuel*, 2021, **305**, 121613.

10 J. Meng, L. Wang, J. Wang, *et al.*, Characterization and Analysis of Molecular-Scale Pore Structure of Coal with Different Metamorphic Degrees, *Energy Fuels*, 2023, **37**, 3634–3653.

11 G. Jia, *Research on Microscopic Pore Structure and Gas Adsorption Characteristics of the Low Rank Coal for*

Aiweiergou Mining Area in Xinjiang with Low-Field NMR, Henan Polytechnic University, 2020.

12 N. Fan, J. Wang, C. Deng, *et al.*, Quantitative characterization of coal microstructure and visualization seepage of macropores using CT-based 3D reconstruction, *J. Nat. Gas Sci. Eng.*, 2020, **81**, 103384.

13 C. Wang, J. Gao and X. Zhang, Effect of Mixed Acid Fluid on the Pore Structure of High Rank Coal and Acid Fluid Optimization, *ACS Omega*, 2022, **7**, 33280–33294.

14 Q. Zhu, Y. Yang, X. Lu, *et al.*, Pore Structure of Coals by Mercury Intrusion, N₂ Adsorption and NMR: A Comparative Study, *Appl. Sci.*, 2019, **9**(8), 1680.

15 Q. Hu, X. Zheng, Q. Li, *et al.*, Pore characteristics and dynamic wetting behavior of coal particles with different particle sizes, *J. Min. & Saf. Eng.*, 2024, **41**, 1058–1068.

16 M. Yang, L. Liu, J. Liu, *et al.*, Study on joint characterization of pore structure of middle-rank coal by nitrogen adsorption-mercury intrusion-NMR, *Coal Sci. Technol.*, 2021, **49**, 67–74.

17 S. Li, X. Wang, C. Fan, *et al.*, Experimental study on evolution characteristics of coal pores under impact loadings, *China Saf. Sci. J.*, 2019, **29**, 91–97.

18 S. Zheng, Y. Yao, D. Liu, *et al.*, Characterizations of full-scale pore size distribution, porosity and permeability of coals: a novel methodology by nuclear magnetic resonance and fractal analysis theory, *Int. J. Coal Geol.*, 2018, **196**, 148–158.

19 Z. Pi, Z. Dong, R. Li, *et al.*, Low-Field NMR Experimental Study on the Effect of Confining Pressure on the Porous Structure and Connectivity of High-Rank Coal, *ACS Omega*, 2022, **7**, 14283–14290.

20 H. Ren, A. Wang, C. Li, *et al.*, Study on porosity characteristics of low-rank coal reservoirs based on nuclear magnetic resonance technology, *Coal Sci. Technol.*, 2017, **45**, 143–148.

21 H. Li, J. Cao, J. Lu, *et al.*, Effect of microwave-assisted cyclic oxidation on the coal internal and surface structure based on NMR and AFM, *Energy*, 2024, **288**, 129872.

22 T. Liu, Multi-field Coupling Processes during Gas Drainage in Deep Fractured Coal Seam and Its Engineering Response, *J. China Univ. Min. Technol.*, 2019, **9**, 28–30.

23 C. Zhai, Y. Sun, Y. Fan, *et al.*, Application and prospect of low-field nuclear magnetic resonance technology in accurate characterization of coal pore structure, *J. China Coal Soc.*, 2022, **47**, 828–848.

24 L. Qin, X. Zhang, J. Matsushima, *et al.*, Accurate characterization method of coal pore and pore throat structure of different coal ranks based on two-dimensional NMR liquid nitrogen fracturing cycles, *Fuel*, 2023, **341**, 127729.

25 Y. Chen, D. Ma, C. Guo, *et al.*, An Experimental Study on the Conductivity Changes in Coal during Methane Adsorption-Desorption and their Influencing Factors, *Acta Geol. Sin.*, 2019, **93**, 704–717.

26 M. Yang, L. Liu, X. Zhang, *et al.*, Nuclear magnetic resonance experimental study on pore structure and fluid characteristics of coal at different ranks, *China Saf. Sci. J.*, 2021, **31**, 81–88.